SUPPLEMENTARY MATERIAL

Characterization of potential probiotic strain, *L. reuteri* B2, and its microencapsulation using alginate-based biopolymers

Mina Popović[1]*, Marijana Stevanović[2], Zlate Velicković[3], Ana Kovacevic[2], Radmila Miljković[2], Nemanja Mirković[4], Aleksandar Marinković[5]

[1]University of Belgrade, Institute of Chemistry, Technology and Metallurgy, National Institute, University of Belgrade, Njegoseva 12, 11000 Belgrade, Serbia, corresponding author

[2]Institute of Virology, Vaccines and Sera, Torlak, Vojvode Stepe 458, 11000 Belgrade, Serbia

[3]Military Academy, University of Defense, Generala Pavla Jurišića - Šturma Street No. 33, 11000 Belgrade, Serbia

[4]Institute of Molecular Genetics and Genetic Engineering, University of Belgrade, Vojvode Stepe 444a, 11000 Belgrade, Serbia

[5]Faculty of Technology and Metallurgy, University of Belgrade, Karnegijeva 4, 11000 Belgrade, Serbia

Keywords: Probiotics, *Lactobacills reuteri*, alginate, starch maleate, microencapsulation

2. Preparation of materials for encapsulation

2.1 Materials

Native wheat starch was purchased from Žito Promet Ruma doo (moisture content ≤15,0%, ash content on d.m. 0.46-0.55%;), while the chemical used for its modification: absolute ethanol and formic acid (≥99.8% and ≥98.0%, respectively; ZORKA Pharma), potassium and sodium hydroxide (≥90.0% and ≥97.0%, respectively; HeMoss, Belgrade), concentrated HCl (Lachema, Czech Republic), diethyl ether (≥99.0%; Fisher UK, Maleic anhydride (MA) Sigma.

2.2 Laboratory isolation of ricinoleic acid (RA)

The isolation of ricinoleic acid (RA) from castor oil was performed analogously to the previously published method [1]: 233 g (0.26 mol) of castor oil and 700 mL of absolute ethanol were placed into a four-neck-reactor equipped with a reflux condenser, mechanical stirrer, thermometer, dropping funnel and nitrogen inlet. After dissolving castor oil, the 30% potassium hydroxide (0.91 mol) was slowly introduced into the reactor with constant stirring. The reaction mixture was maintained at approximately 10 °C during the addition of potassium hydroxide for 1 h. Hereafter, the reaction mixture was heated to 50 °C and the temperature was kept constant for 2 h. After that, two-thirds of the solvent was removed from the mixture by distillation at atmospheric pressure. The obtained slurry was dissolved in distilled water, acidified with concentrated HCl to pH 3.0, purified with activated carbon, and filtered. The obtained (RA) was extracted by diethyl ether and the obtained solution was dried with anhydrous sodium sulfate, and then in a vacuum dryer at 80 ^{o}C/2000 Pa for 5 h. The FTIR spectrum was presented in *section 3.1*. Elemental analysis calculated for $C_{18}H_{34}O_3$ (M_w = 298.46 gmol^{-1}): C, 71.42; H, 10.32; O, 18.26. Found: C, 70.98; H, 10.31; O, 18.71. The oxygen percent was calculated as the difference to 100%. NMR analysis **(Fig. S1.)**: ^{1}H-NMR (200 MHz, $CDCl_3$-d_6, δ / ppm): 0.88 (3H, s, $C_{18}H_3$), 1.31-1.35 (16H, m, *J* = 11.0 Hz, $C_{4\text{-}7}$, $C_{14\text{-}17}$H), 1.44 (2H, m, J = 11.0 Hz, C_{13}H), 1.62 (2H, m, J = 7.0 Hz, C_3H), 2.03 (2H, m, J = 7.0 Hz, C_8H), 2.22 (2H, m, J = 7.0, C_{11}H), 2.33 (2H, dd, C_2H), 3.63 (1H, m, C_{12}H), 5.39-5.53 (2H, m, C_9H and C_{10}H), 6.5 (1H, s, C_{12}OH), 9.65 (1H, s, C_1OH); ^{13}C-NMR (50 MHz, DMSO–d6, δ / ppm): 14.0 (C_{18}), 22.6 (C_{17}), 25.5 (C_{14} and C_3), 28.9-

29.3 (C_{4-7} and C_{15}), 32.0 (C_{16}), 35.0 (C_2), 37.0 (C_{11} and C_{13}), 71.7 (C_{12}), 125 (C_{10}), 133 (C_9), 179 (C_1).

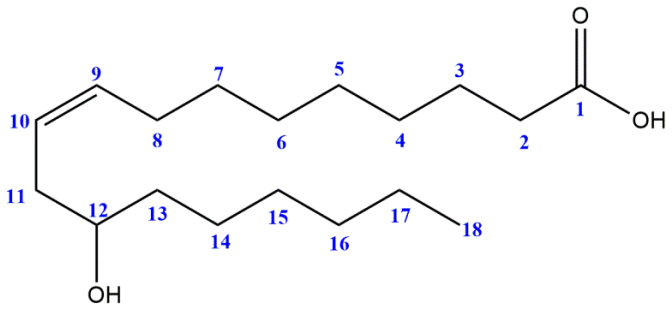

Figure S1. NMR analysis of ricinoleic acid

2.3 Laboratory preparation of starch maleate (SM) monoester

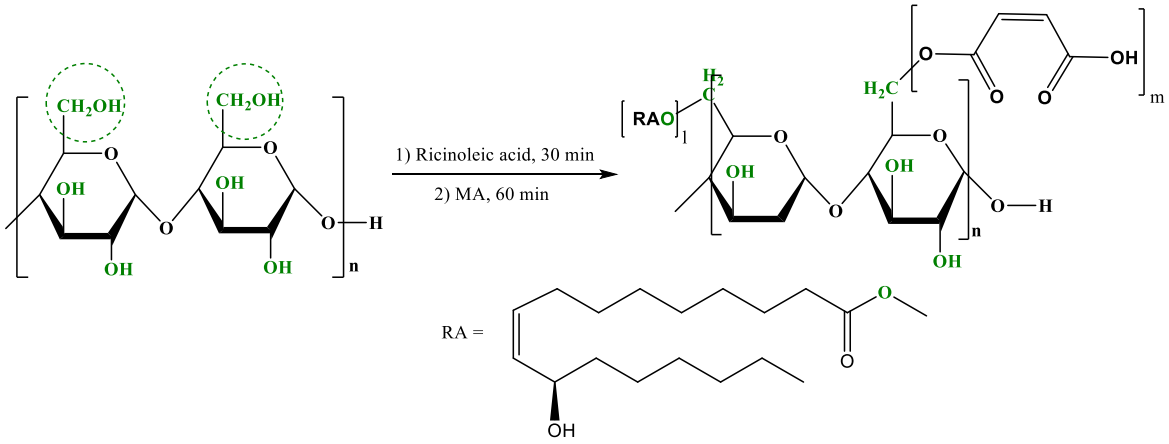

Figure S2. Proposed mechanism of starch modification with MA to obtain SM

Table S1. Quantities of reactants and reaction conditions applied for production starch maleate

Experiment	Starch, [kg]	RA [mL]	MA [kg]	T, [°C]*
1	1		0.8	80
2	1		0.6	80
3	1		0.4	80
4	1		0.3	80
5	1	40	0.8	80
6	1	40	0.6	80
7	1	40	0.4	80
8	1	40	0.3	80
9	1	60	0.4	80

* temperature of the process in the second stage

2.4 Characterization

The viscosity of selected modified starch obtained at the laboratory level was determined using a capillary viscometer (Cannon-Fenske viscometer, CF Method) following Method 1 [2].

Fourier-transform infrared spectroscopy (FTIR) was used for the characterization of the materials (Na-alg and Na-alg+SM), that were used for encapsulation of *L. reuteri* B2. Tests were performed using a Nicolet iS10 spectrometer (Thermo Scientific) in the attenuated total reflectance (ATR) mode with a single bounce 45 °F Golden Gate ATR accessory with a diamond crystal, and DTGS detector. FTIR spectra were obtained at 4 cm^{-1}resolution with ATR correction. The FTIR spectrometer was equipped with OMNIC software and recorded the spectra in the wavelength range from 2.5 μm to 20 μm (i.e., 4000 –500 cm^{-1}). An examination using FTIR spectroscopy was performed to determine the presence of functional groups and the interaction between the materials in the microsphere formula. The FTIR spectra of materials are illustrated in Figure 2.

The thermal analysis of the microsphere was performed through thermogravimetric (TG) and differential scanning calorimetry analysis (DSC) with SDT Q600 simulated TGA-DTA instrument - TA Instruments, for studying the thermal properties of oxidized starches. Samples were heated to 600 °C (10 °C min^{-1}) under a dynamic nitrogen atmosphere flowing at 20 mL min^{-1}.

Determination of Na-alg – Na-alg+SM beads size distribution: Samples of Na-alg beads and Na-alg+SM beads were taken randomly and were measured with digital calipers (ROHS CE Digital Caliper–SH 20, China) to determine their size at pH 2.5 after 2 hours.

Optical microscopy was used to characterize filled and unfilled alginate beads. A microscope (Motic BA210) with 100x objective lenses was used to capture images of the beads. Alginate suspensions were vortexed to separate individual beads. All optical images were taken using a digital camera (Moticam 1SP 1.3 MP) and then characterized using the instrument software (Motic Images Plus 2.0) (Figure 3).

To determine and characterize the microstructure of the beads from, Na-alg and Na-alg+SM with and without *L. reuteri* B2 strains, it was used a scanning electron microscope (Tescan Mira3 XMU FE-SEM) operated at 20 kV. To prepare the samples before analysis, calcium alginate beads were air-dried at room temperature for at least 24 hours on Petri dishes. Subsequently, the beads were spattered with 10 nm gold and mounted on an aluminum stud,

which was loaded into the microscope. Images of the calcium alginate beads were recorded in randomly selected fields. Before analysis, oxidized starch products were coated with Au. (Figure 4).

The degree of substitution (DS) of the prepared samples of starch maleate (SM) is determined using the method described by Tay et al.[3] The degree of the substitution was determined with the following formula:

$$DS = \frac{162 \times n_{COOH}}{m - 99 \times n_{COOH}} \quad \text{(S1)}$$

where: 162 g/mol – molar mass of unsubstituted anhydroglucose unit, 99 g/mol is the net increase in the mass of an AGU for each maleate molecule substituted, m is the weight of sample analyzed, and nCOOH is the amount of COOH calculated from the average titrated volume of standard HCl according to Equation (S2):

$$n_{COOH} = V_{NaOH} c_{NaOH} - V_{HCl} c_{HCl} \quad \text{(S2)}$$

Reaction efficiency was calculated according to Equation (S3):

$$\text{RE}(\%) = \frac{\text{DS} \times \text{mole of anhydroglucose unit}}{\text{mole of maleic anhydride}} \times 100 \quad \text{(S3)}$$

Ester value was determined according to standard test method ASTM D1617 - 07(2012) (Standard Test Method for Ester Value of Solvents and Thinners). Acid value determination was performed according to ASTM D664.

The swelling capacity (SC) and solubility (S) of SM relate to the intensity of intermolecular interactions in the amorphous and crystalline domain [4]. The SC quantitatively expresses the capability of the modified domain of starch to hydrate and S describes the percentage of the highly modified starch macromolecules leached from the granules after swelling.

Swelling capacity (SC) and solubility (S) of the samples were determined according to Zhou, J. et al. (2016) [5]**.** In a typical experiment, a 0.2 g sample was put into a 100 mL beaker, and then 20 mL deionized water was mixed using ultrasound treatment (Bandelin SONOREX, Ultrasonic bath, Germany) at 100% power with continuous stirring for 30 min in a water bath at 40 °C. The obtained suspension was centrifuged at 4250 rpm for 10 min. To measure the SC and S, supernatant and sediment were carefully transferred into Petri dishes respectively and dried overnight in a hot air oven at 105 °C. The SC and S were calculated as:

$$SC = \frac{W_2 - W_1}{W_0} \quad \text{(S4)}$$

$$S, \% = \frac{W_3}{W_3 + W_0} \times 100 \quad \text{(S5)}$$

where W_0 is the weight of sediment on a dry basis, $W_1$is the weight of the centrifugal tube, W_2 is the weight of the centrifugal tube with swollen sediment, and W_3 is the weight of supernatant on a dry basis.

The native and modified starches were dried at 60 °C for three days to eliminate moisture from the grains. Afterward, 1.0 g of each type of starch was weighed and placed in an environment with 90% relative humidity for 24 h. After this time, the samples were weighed again. The amount of moisture absorbed was calculated gravimetrically by Equation (S6) [6]:

$$MAd, \% = \frac{W_i - W_0}{W_0} \times 100 \quad \text{(S6)}$$

where W_0 is the weight of dry samples and W_0 is the weight of samples after moisture absorption.

The moisture content (MC) of the different samples was determined by weighing 0.5 g of native and modified starches and dried in an oven at 100°C for 24 h. The percentage of moisture content was calculated with the following Equation (S7) [7]:

$$MC, \% = \frac{m_w - m_d}{m_d} \times 100\% \quad \text{(S7)}$$

where m_w is the mass of the wet sample and m_d is the mass of the dried sample.

2.12 Statistical analysis

The concept of hypothesis testing was reinforced by explaining the null hypothesis, or the hypothesis of no difference and alternative hypotheses. In the activity that was developed, one null hypothesis was that the diameters of zones from antibiotic inhibition would that those diameters would not be different regardless of the person making the measurement. The appropriate statistical test, either the t-test or ANOVA, was applied to test each null hypothesis, as noted. The t-test is a powerful and robust test for determining if two populations have different means when samples are independent and random and the measured variable is continuous and normally distributed. ANOVA is more appropriate (and less error-prone) than running multiple t-tests when there are more than two samples to compare. In ANOVA there are two types of variance to consider: error variance (within-groups variance) and treatment variance (between-groups variance). Since the zones of inhibition being measured by each group member are the same, the within-groups variance should be the same. Therefore, any difference between the

variances of the measurements would be due to the treatment (in this activity, the individual making the measurement). ANOVA can indicate a difference between the treatments but additional tests are necessary to find which treatments are significantly different. An alpha value of 0.05 was used for all analyses. This is the level usually selected as it offers a good compromise to avoid Type I (rejecting a true null hypothesis) or Type II (not rejecting a false null hypothesis) errors.

Statistical tools are used to collect, organize, analyze, and interpret numerical data. Descriptive statistics allow investigators to summarize large amounts of data to more understandable levels using numerical descriptors (e.g.. mean, mode, median, or standard deviation) or graphical methods.

3. Results

3.3 Antimicrobial activity

The mean values of the inhibition zones depending on the evaluator are given in **Figure S3,** and the results of descriptive statistics of inhibition zone measurements for different pathogenic microorganisms are given in Table S3.

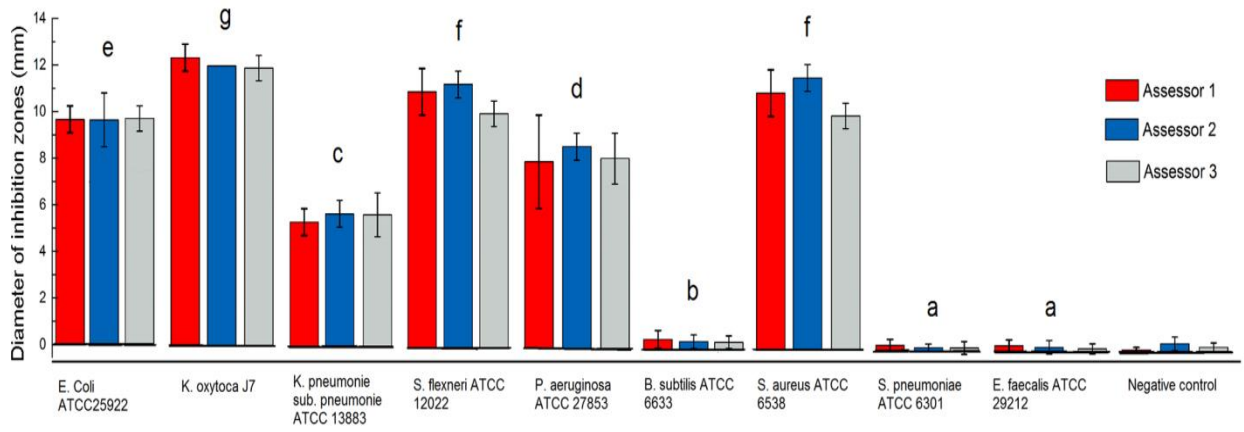

Figure S3. *In vitro* antibacterial activity of *L. reuteri* B2 to various foodborne pathogens. Antibacterial activities of the cultured supernatant against 9 kinds of pathogenic bacteria. Symbols with a different letter (a–f) are significantly different at $P < 0.05$. Error bars represent SD

Table S3. Statistical processing of inhibition zone* measurement data using JASP

	E. Coli ATCC 25922	*K. oxytoca J7*	*K. pneumonie sub. pneumonie ATCC 13883*	*S. flexneri ATCC 12022*	*P. aeruginosa ATCC 27853*	*B. subtilis ATCC 6633*	*S. aureus ATCC 6538*	*S. pneumoniae ATCC 6301*	*E. faecalis ATCC 29212*	Negative control
Valid	9	9	9	9	9	9	9	9	9	9
Mean	9.889	12.333	5.667	11	8.444	0.367	11.111	0.2	0.178	0.2
Std. Error of Mean	0.261	0.167	0.236	0.236	0.412	0.094	0.261	0.071	0.076	0.073
Median	10	12	6	11	8	0.5	11	0.2	0	0.2
Mode	10	12	5	11	8	0.5	11	0	0	0
Std. Deviation	0.782	0.5	0.707	0.707	1.236	0.283	0.782	0.212	0.228	0.218
Variance	0.611	0.25	0.5	0.5	1.528	0.08	0.611	0.045	0.052	0.048
Shapiro-Wilk	0.838	0.617	0.805	0.833	0.889	0.778	0.838	0.823	0.741	0.81
P-value of Shapiro-Wilk	0.055	< .001	0.024	0.049	0.195	0.011	0.055	0.038	0.004	0.026
Range	2	1	2	2	4	0.7	2	0.5	0.5	0.5
Minimum	9	12	5	10	6	0	10	0	0	0
Maximum	11	13	7	12	10	0.7	12	0.5	0.5	0.5

* total data of all assessors

3.5 SM characterization

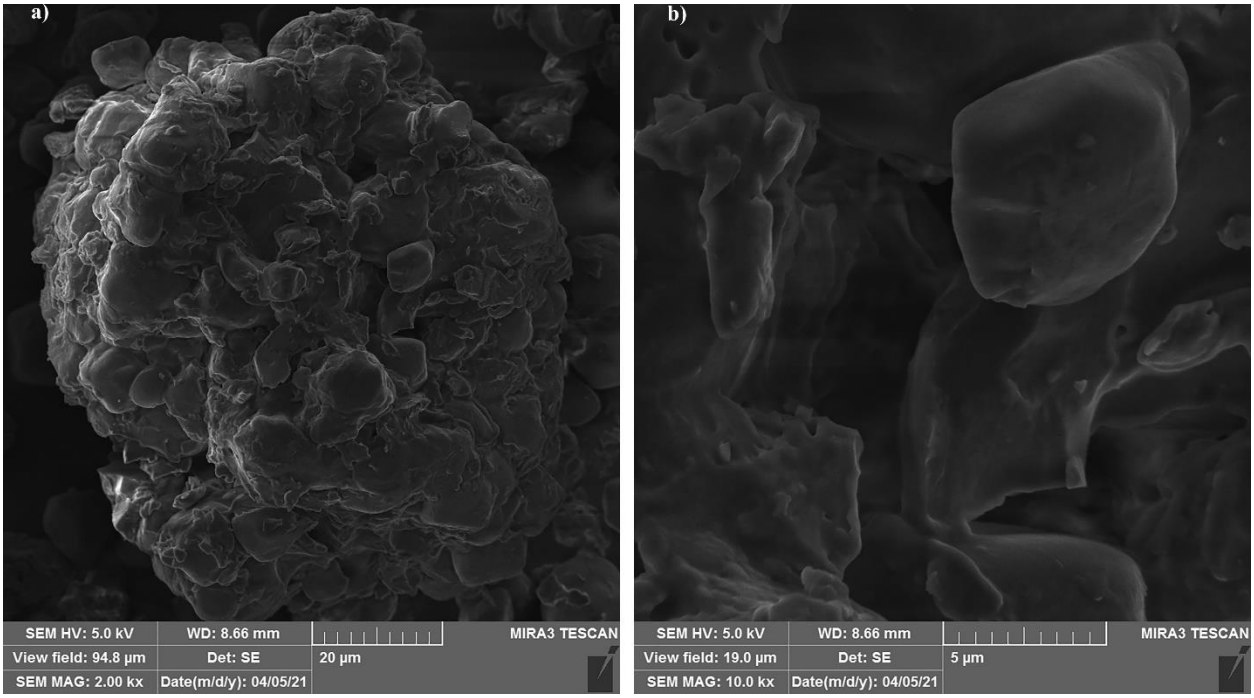

Figure S4. SEM micrograph of starch maleate on a) 2.0 kx and b) 10.0 kx magnifications

3.6 Optimization of encapsulation yield

Since the synthesis process is very complex and a fixed initial reactants molar ratio is taken and other variables that affect the encapsulation process were used in the statistical design of the experiment. Hence, the developed cubic model of encapsulation yield dependence on the reaction conditions of synthesis in terms of encoded factors manages:

$$X=+65.86+21.94*A-5.84*B+1.35*AB-8.97*A^2-4.42*B^2-0.61*A^2B-2.10*AB^2-17.49*A^{\wedge 3}+5.27*B^3$$

In this model, negative coefficients corresponded to unfavorable effects on the encapsulation yield for B, A^2, B^2, $AB^{2,}$ and A^3, whilst positive coefficients corresponded to favorable effects on the encapsulation yield for A, AB, and B^3. Parameters with coefficients close to zero indicated a lower effect on the encapsulation yield than that of larger coefficients under the same magnitude of change in that certain factor. Thus, A^2B did not significantly affect the encapsulation yield when these factors were changed accordingly

For checking the adequacy of the developed models at 95% confidence level ANOVA technique is used[8–10]**.** ANOVA results for the response surface quadratic models are given in Table S4. The criteria followed in this technique is that if the calculated value of the F-ratio of the regression model is more than the standard value specified (F-table) for 95% confidence level, and then the model is considered adequate within the confidence limit[10]. From Table S4, it is observed that all the models satisfy the adequacy conditions in a non-linear form. The Model F-value of 18.56 implies the model is significant. There is only a 0.01% chance that a "Model F-Value" this large could occur due to noise. Values of "Prob > F" less than 0.0500 indicate model terms are significant. In this case, A, A^2, B^2, A^3 are significant model terms. Values greater than 0.1000 indicate the model terms are not significant. If there are many insignificant model terms (not counting those required to support hierarchy), model reduction may improve a model. In addition to verification through ANOVA technique, using the Design-Expert, Software Version 9 Models were validated by conducting experiments with a new set of parameters and the multiple responses.

Table S4. Variance Analysis (ANOVA) for the surface cubic model of the response to encapsulation yield

Source	Sum of Squares	df	Mean Square	F Value	p-value Prob > F	
Model	794.37	9	88.26	18.56	0.0010	significant
A-content Na alginate	*140.72*	*1*	*140.72*	*29.59*	*0.0016*	significant
B-Solution starch maleate	*10.17*	*1*	*10.17*	*2.14*	*0.1940*	
AB	*4.50*	*1*	*4.50*	*0.95*	*0.3684*	
A^2	*203.99*	*1*	*203.99*	*42.90*	*0.0006*	significant
B^2	*43.83*	*1*	*43.83*	*9.22*	*0.0229*	significant
A^2B	*0.46*	*1*	*0.46*	*0.096*	*0.7667*	
AB^2	*4.23*	*1*	*4.23*	*0.89*	*0.3819*	
A^3	*79.57*	*1*	*79.57*	*16.73*	*0.0064*	significant
B^3	*8.13*	*1*	*8.13*	*1.71*	*0.2389*	
Residual	28.53	6	4.75			
Lack of Fit	*28.53*	*1*	*28.53*			
Pure Error	*0.000*	*5*	*0.000*			
Cor Total	822.90	15				

Model assessment	
Std. Dev.	2.18
Mean	58.04
C.V. %	3.76
PRESS	128.67
R^2	0.9653

The prediction of the maximum yield encapsulation relative to the content Na-alg and SM solution is shown graphically in Figure S5.

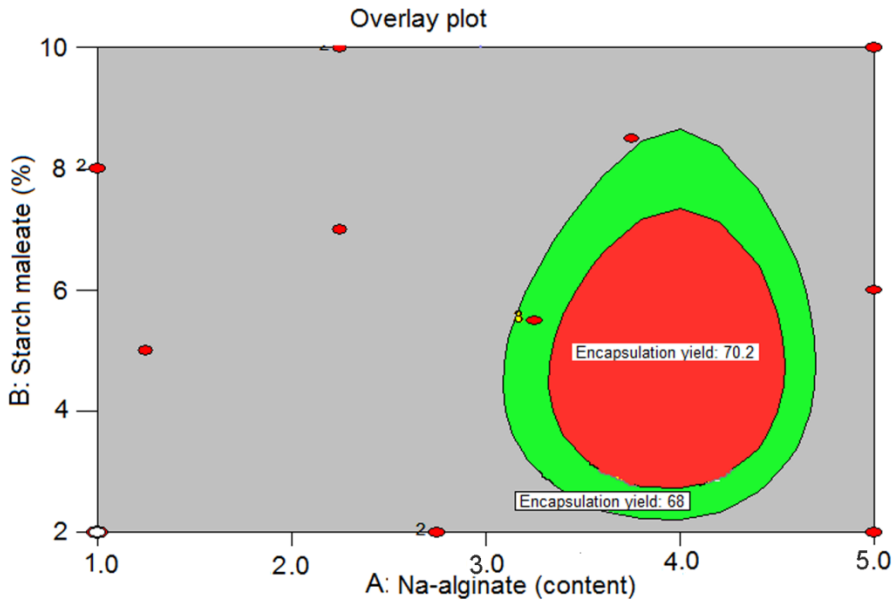

Fig. S5 View Optimal Reaction Conditions for Maximum Yield encapsulation (overlay plot)

3.7 Size distribution of alginate beads in acidic conditions

Graphical representation of statistics for the results of particle size and mass measurements is given in Figures S6-S9.

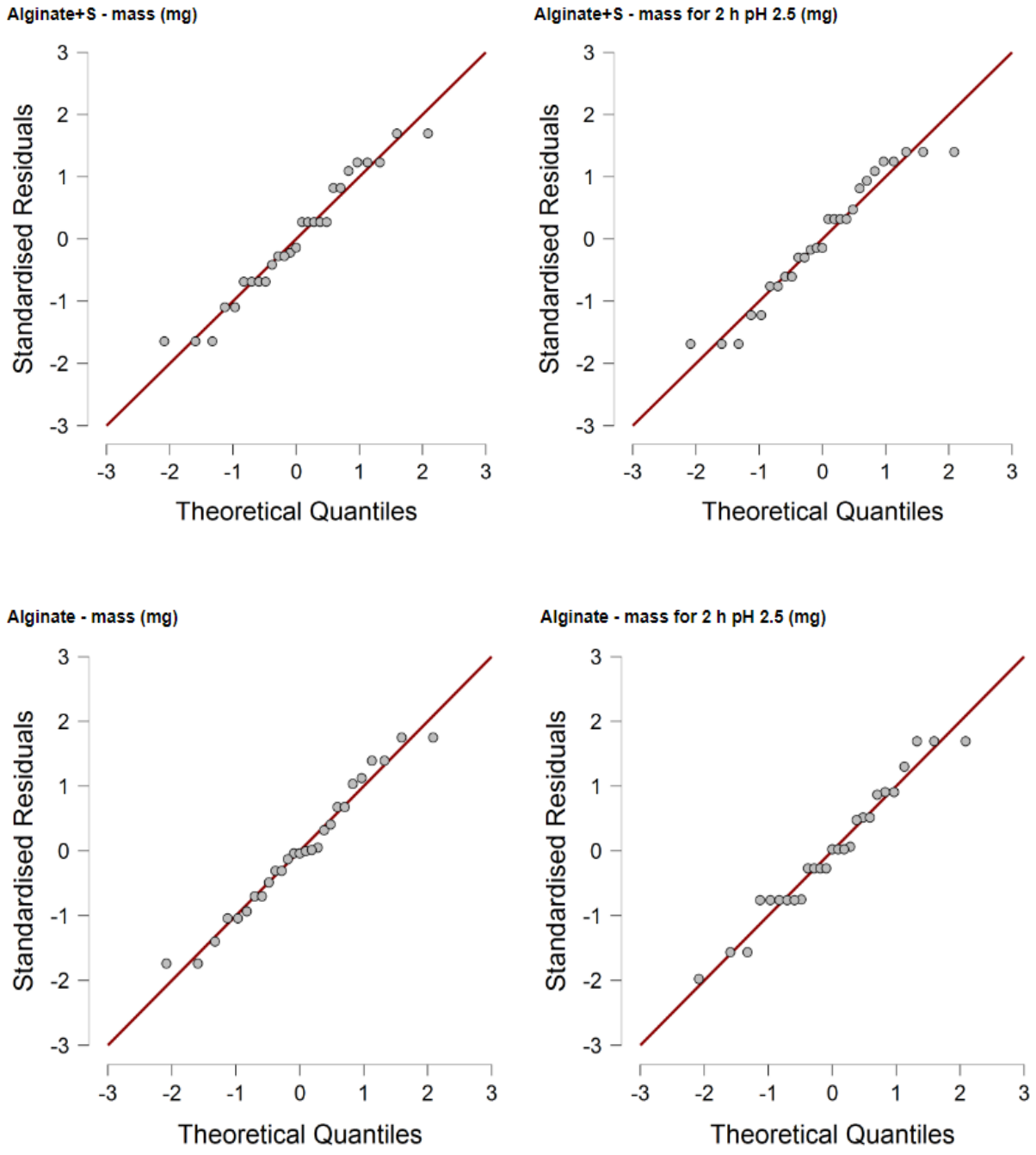

Figure S6 Q-Q plot of Alg and Alg/S-MA beads mass at neutral and pH 2.5 after 2h soaking

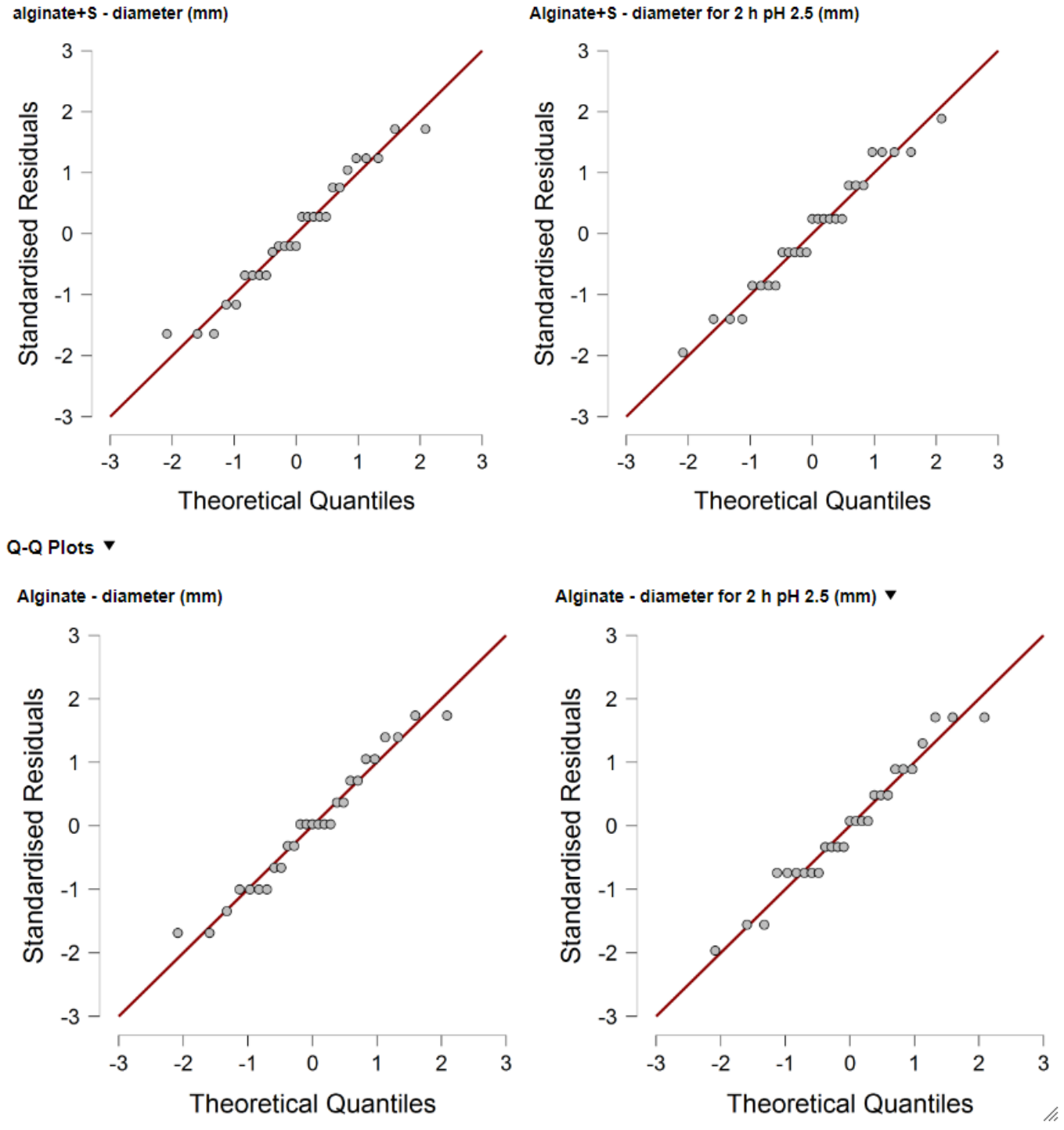

Figure S7 Q-Q plot of Alg and Alg/S-MA beads diameter at neutral and pH 2.5 for 2h soaking

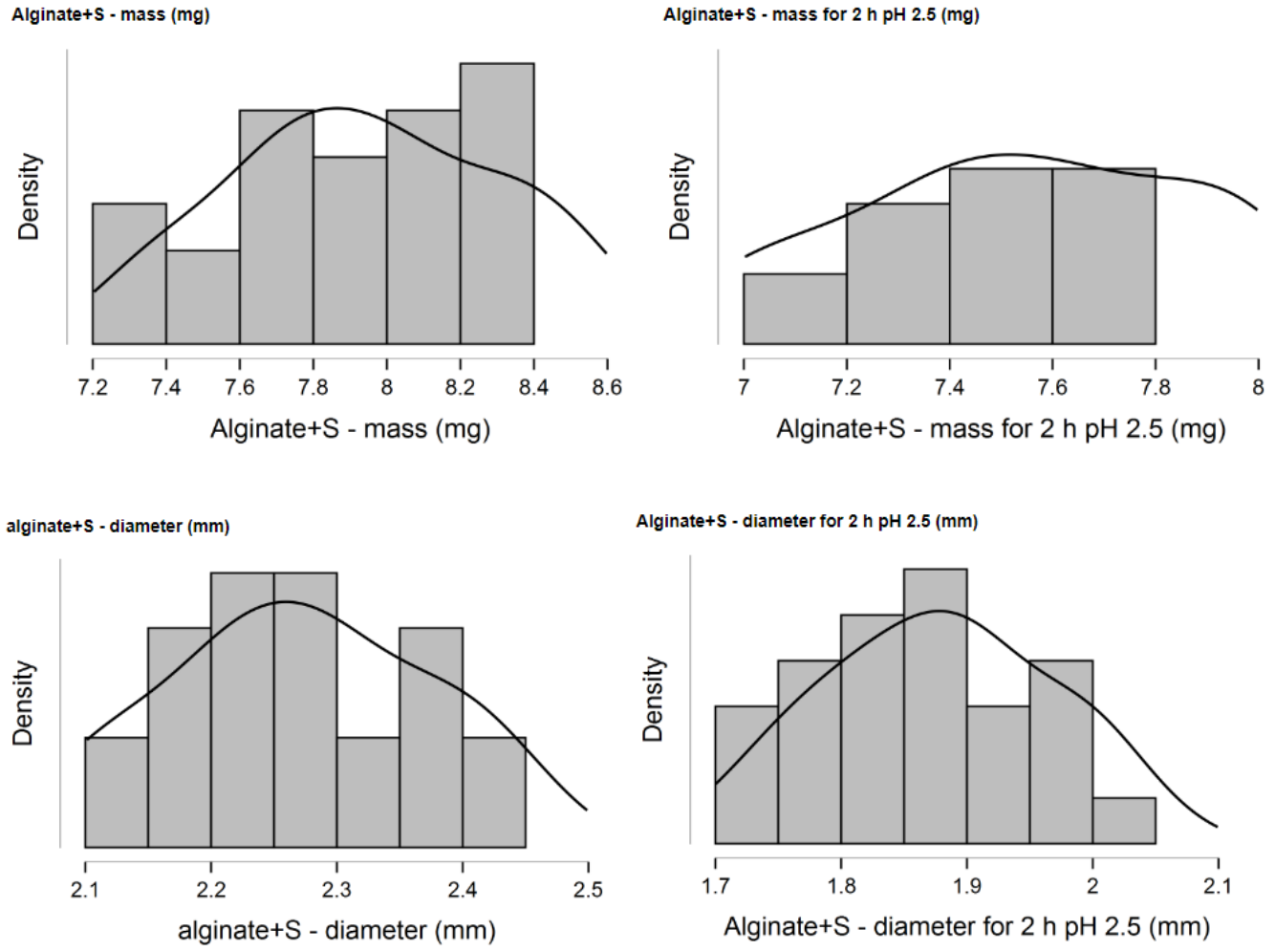

Figure S8 Plot of density versus diameter for Na-alg and Na-alg+SM beads diameter at neutral and pH 2.5 for 2h soaking

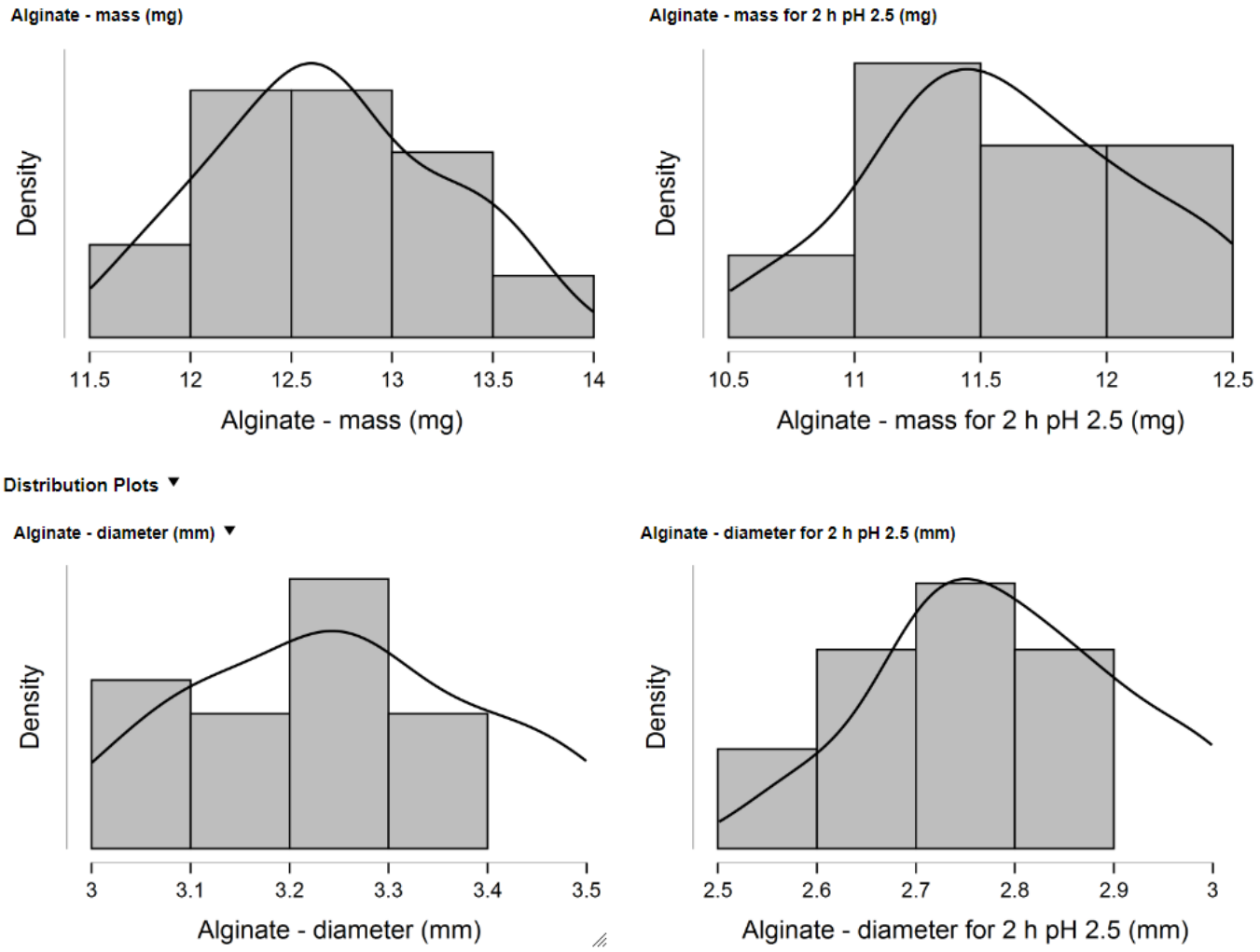

Figure S9 Plot of density versus mass for Alg and Alg/S-MA beads mass at neutral and pH 2.5 for 2h soaking

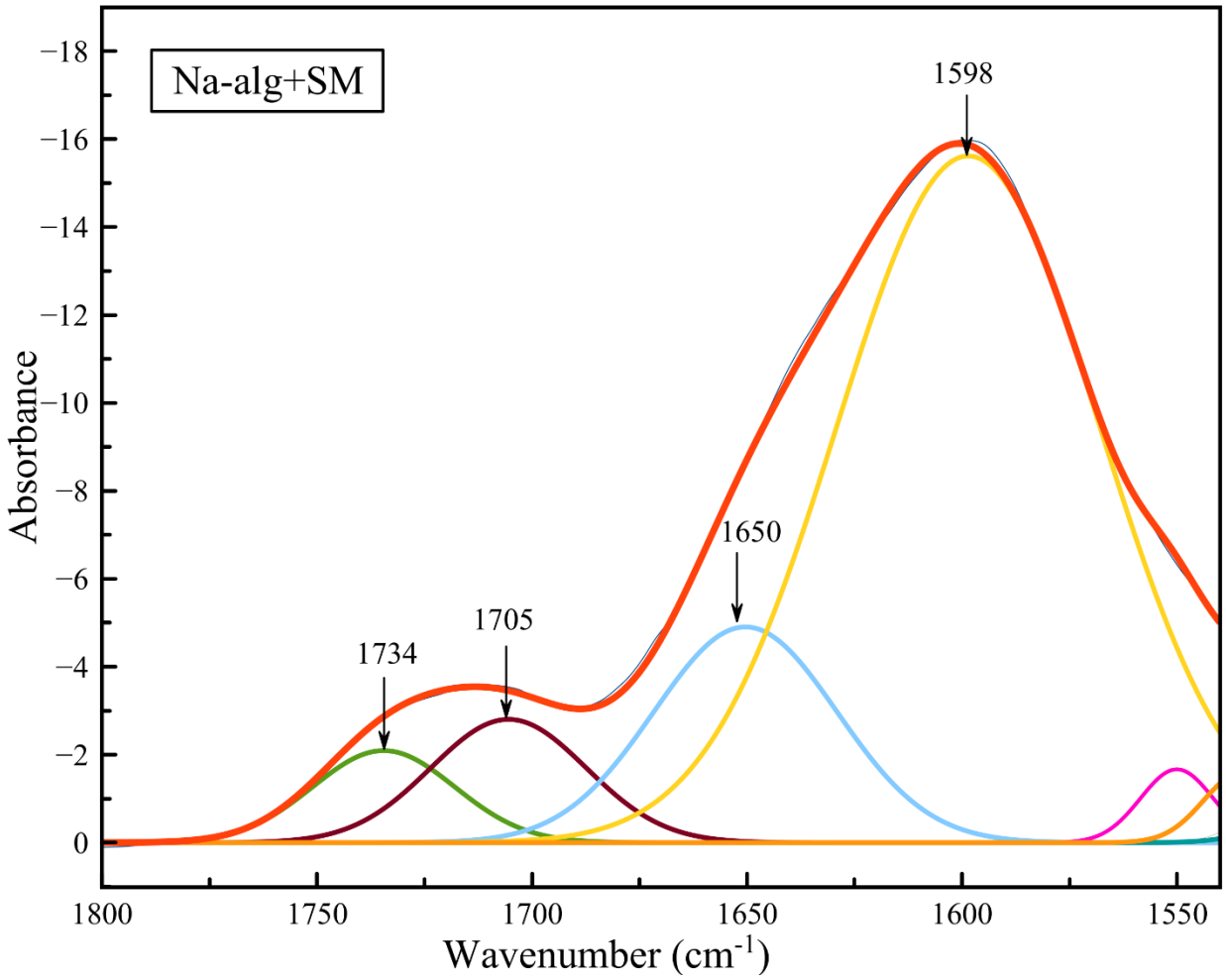

Figure S10. Deconvolution of FTIR spectrum of Na-Alg+SM in the region from 1540 to 1800 cm^{-1}

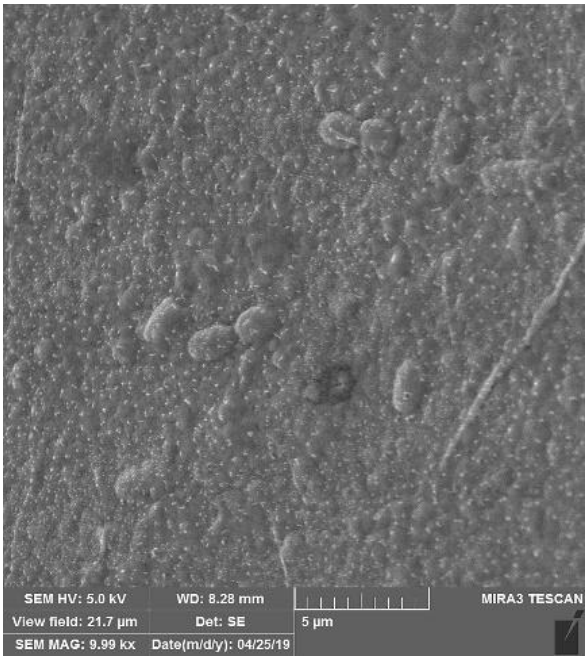

Figure S11. SEM micrograph of Na-alg + SM beads with *L. reuteri* B2 cells at 10kx magnification

References

[1] Karić N, Rusmirović J, Dolić M, Kovačević T, Pecić L, Radovanović Ž, et al. Preparation and properties of hydrogen peroxide oxidized starch for industrial use. Hem Ind 2020;74:D1–8. https://doi.org/10.2298/HEMIND190722004K.

[2] The United States Pharmacopeial Convention S. The United States Pharmacopeial Convention Methylcellulose. United States Pharmacopeial Conv 2014:1–2.

[3] Tay SH, Pang SC, Chin SF. Facile synthesis of starch-maleate monoesters from native sago starch. Carbohydr Polym 2012;88:1195–200. https://doi.org/10.1016/j.carbpol.2012.01.079.

[4] Zhang P, Whistler RL, BeMiller JN, Hamaker BR. Banana starch: production, physicochemical properties, and digestibility—a review. Carbohydr Polym 2005;59:443–58. https://doi.org/10.1016/j.carbpol.2004.10.014.

[5] Zhou J, Tong J, Su X, Ren L. Hydrophobic starch nanocrystals preparations through crosslinking modification using citric acid. Int J Biol Macromol 2016;91:186–1193. https://doi.org/10.1016/j.ijbiomac.2016.06.082.

[6] Bergel BF, Dias Osorio S, da Luz LM, Santana RMC. Effects of hydrophobized starches on thermoplastic starch foams made from potato starch. Carbohydr Polym 2018;200:106–14. https://doi.org/10.1016/j.carbpol.2018.07.047.

[7] Seligra PG, Medina Jaramillo C, Famá L, Goyanes S. Biodegradable and non-retrogradable eco-films based on starch-glycerol with citric acid as crosslinking agent. Carbohydr Polym 2016;138:66–74. https://doi.org/10.1016/j.carbpol.2015.11.041.

[8] Iqbal M, Iqbal N, Bhatti IA, Ahmad N, Zahid M. Response surface methodology application in optimization of cadmium adsorption by shoe waste: A good option of waste mitigation by waste. Ecol Eng 2016;88:265–75. https://doi.org/10.1016/j.ecoleng.2015.12.041.

[9] Karanac M, Đolić M, Veličković Z, Kapidžić A, Ivanovski V, Mitrić M, et al. Efficient multistep arsenate removal onto magnetite modified fly ash. J Environ Manage 2018;224:263–76. https://doi.org/10.1016/j.jenvman.2018.07.051.

[10] Xiyili H, Çetintaş S, Bingöl D. Removal of some heavy metals onto mechanically

activated fly ash: Modeling approach for optimization, isotherms, kinetics and thermodynamics. Process Saf Environ Prot 2017;109:288–300. https://doi.org/10.1016/j.psep.2017.04.012.